Random Field Ising Models: Fractal Interfaces and their Implications

A Bupathy[1], M Kumar[2], V Banerjee[1] and S Puri[2]

[1] Department of Physics, Indian Institute of Technology, New Delhi – 110016, India.
[2] School of Physical Sciences, Jawaharlal Nehru University, New Delhi – 110067, India.

E-mail: varsha@physics.iitd.ac.in

Abstract. We use a computationally efficient graph-cut (GC) method to obtain exact ground-states of the $d = 3$ random field Ising model (RFIM) on simple cubic (SC), body-centered cubic (BCC) and face-centered cubic (FCC) lattices with Gaussian, Uniform and Bimodal distributions for the disorder Δ. At small-r, the correlation function $C(r, \Delta)$ shows a cusp singularity characterised by a non-integer roughness exponent α signifying rough fractal interfaces with dimension $d_f = d - \alpha$. In the paramagnetic phase ($\Delta > \Delta_c$), $\alpha \simeq 0.5$ for all lattice and disorder types. In the ferromagnetic phase ($\Delta < \Delta_c$), $\alpha \simeq 0.66$ with minor variations for the different lattice types. Our predictions are confirmed by scattering data from diluted antiferromagnets (DAFFs). Fractal interfaces have important implications on growth and relaxation.

1. Introduction

The random field Ising model (RFIM) is one of the simplest models that provides a framework to study the effects of quenched disorder and randomness on static and dynamic properties. It is realized by many physical systems such as dilute antiferromagnets in a field (DAFFs) [1], diluted dipolar magnet $LiHo_xY_{1-x}F_4$ [2], relaxor ferroelectrics [3], colloid-polymer mixtures [4], non-equilibrium phenomena like Barkhausen noise in magnetic hysteresis [5], etc. The RFIM comprises of N Ising spins on a d-dimensional lattice with the Hamiltonian given by [6]:

$$\mathcal{H}(\{\sigma_i\}) = -J \sum_{\langle ij \rangle} \sigma_i \sigma_j - \sum_i h_i \sigma_i, \quad \sigma_i = \pm 1 \tag{1}$$

Here, $J > 0$ is the strength of the nearest neighbour coupling and promotes ferromagnetic order and h_i's are the disordering random fields usually drawn from one of the following distributions:

$$\text{Gaussian} : P_1(h_i) = \frac{1}{2\pi\Delta^2} e^{-h_i^2/(2\Delta^2)}, \tag{2}$$

$$\text{Uniform} : P_2(h_i) = \begin{cases} \left[\sqrt{12}\Delta\right]^{-1} & : |h_i| \leq \sqrt{3}\Delta, \\ 0 & : |h_i| > \sqrt{3}\Delta, \end{cases} \tag{3}$$

$$\text{Bimodal} : P_3(h_i) = \frac{1}{2}\left[\delta(h_i - \Delta) + \delta(h_i + \Delta)\right]. \tag{4}$$

The standard deviation Δ is a measure of the strength of disorder. All the three distributions have mean zero and variance Δ^2. As the disorder strength is increased, the system undergoes a transition from the ferro to para phase at a critical disorder strength Δ_c.

The presence of competing interactions gives rise to a complex free energy landscape having several local minima separated by energy barriers that grow exponentially with N. The evolving system therefore gets trapped in a local minimum which can be arbitrarily far from the global minimum. As a result there is a multitude of time-scales which lead to slow growth and anomalous relaxation. Such energy functions are very difficult to minimize. Traditional Monte Carlo (MC) procedures such as the Metropolis algorithm or parallel tempering involve only $O(1)$ spin flips at a time and are unable to approach the ground state (GS). In recent years, several sophisticated techniques based on max-flow/min-cut or graph-cut (GC) methods have been employed to study the RFIM [7]. These methods attempt to find a local minimum by a simultaneous re-labeling of a large number of spin variables. An exponentially large portion of the phase-space can be sampled in one move, thereby facilitating a quick search for the global minimum. Further, the RFIM Hamiltonian satisfies a *regularity condition* which guarantees the GS via the GC.

The random fields cause pinning and roughening of interfaces. They are then characterized by a roughness exponent α which is related to the fractal dimension $d_f = d - \alpha$. When is the interfacial texture consequential? Consider a thermal quench from a high temperature paramagnetic phase to a low temperature ferromagnetic phase. The evolution of the system is via the motion of interfaces due to surface tension, but is impeded by the presence of energy barriers due to the disordering fields. The domain growth therefore is due to thermally activated barrier hopping. According to Villain [8], the barrier energy in the RFIM is $E_B \sim R^m$ where R is the characteristic length scale in the system and the barrier exponent $m = 2-\alpha$. Consequently, this class of disordered systems exhibits slow *logarithmic growth* [9]. On a related note, de-pinning of interfaces on application of an external field has generated technological interest [10, 11]. The creep motion that preceeds the de-pinning transition is greatly affected by the interfacial roughness.

In this paper, we obtain GS morphologies ($T = 0$) of the RFIM on: (i) simple cubic (SC), body-centered cubic (BCC) and face-centered cubic (FCC) lattices with Gaussian disorder and (ii) SC lattice with Gaussian (G), Uniform (U) and Bimodal (B) distributions, by a computationally efficient GC protocol introduced by Boykov and Kolmogorov (BK) [12]. It's polynomial time complexity of O(N) enabled us to access ground states of substantially larger system sizes than in previous studies which used procedures with complexity of O(N^3) and more. We analyze the textures of GS morphologies using the correlation function $C(r, \Delta)$ and the structure factor $S(k, \Delta)$. The main results of our paper are as follows:
(a) The GS morphologies comprise of correlated domains of "up" spins and "down" spins separated by rough interfaces. These correlated regions grow in size as the disorder strength $\Delta \to \Delta_c^+$.
(b) By evaluating the Binder cummulant, our estimates of the critical disorder Δ_c are (a) 2.278 ± 0.002 (SC, G), (b) 3.316 ± 0.002 (BCC, G), (c) 5.16 ± 0.002 (FCC, G), (d) 2.234 ± 0.002 (SC, U) and (e) 2.20 ± 0.002 (SC, B).
(c) At small-r, the correlation function $C(r, \Delta)$ shows a cusp singularity with distinct roughness exponents α for the ferromagnetic phase ($\Delta < \Delta_c$) and paramagnetic phase ($\Delta > \Delta_c$). The structure factor $S(k, \Delta)$ correspondingly shows a non-Porod tail signifying scattering off fractal interfaces.
(d) In the paramagnetic phase ($\Delta > \Delta_c$), the roughness exponent $\alpha = 0.5 \pm 0.01$ for all three lattice types and disorder distributions, showing that the interfacial properties are universal.
(e) In the ferromagnetic phase ($\Delta < \Delta_c$), the roughness exponent $\alpha \simeq 0.66$ with minor variations for the different lattice types. Though tiny, these variations have important implications.

(f) We explain the non-Porod behavior of the structure factor obtained in small-angle neutron-scattering experiments on dilute antiferromagnets.

This paper is organized as follows. In Sec. 2 we present the GC procedure used to obtain the ground states and the tools for characterizing these morphologies. In Sec. 3, we analyze the RFIM morphologies obtained for the SC, BCC and FCC lattices. We also verify our predictions of fractal interfaces in a large number of dilute antiferromagnets by studying the small-angle neutron scattering data. Finally, we conclude this paper with a summary and discussion in Sec. 4.

2. Methodology

2.1. Graph Cuts for Energy minimization

In the GC method, the spin lattice is represented as a graph $\mathcal{G}$ with vertices $\mathcal{V}$ and edges $\mathcal{E}$ connecting them. Each vertex i is assigned a label $s_i \in \mathcal{L}$. The energy function associated with such a labelling is given as

$$E(\{s_i\}) = \sum_{\{ij\}\in\mathcal{N}} V_{ij}(s_i, s_j) + \sum_i D_i(s_i). \tag{5}$$

Here, V_{ij} is the *weight* of edge ij and represents the penalty of assigning labels s_i and s_j to vertices i and j respectively, and D_i is the cost of assigning the label s_i to vertex i. For simplicity, we only discuss the case of binary labels, i.e., $\mathcal{L} = \{0, 1\}$. A partitioning of the vertices $\mathcal{V}$ into two sets $\mathcal{S}$ and $\mathcal{T}$, then corresponds to labelling the vertices and is called a *cut* $\mathcal{C}$. Any edge $ij \in \mathcal{E}$ with $i \in \mathcal{S}$ and $j \in \mathcal{T}$ (or vice versa) is a cut edge. The cost of the cut is the sum of the weights of the cut edges. The problem is then to find the cut with the smallest cost or *min-cut*.

The RFIM Hamiltonian belongs to a special class of energy functions which satisfies a *regularity condition* [13]. The latter assures convergence to *exact* ground states if energy minimization is via graph-cuts. In recent papers [14, 15], we have described in detail our application of the Boykov-Kolmogorov GC method (BK-GCM) [12] to the RFIM. For the sake of brevity, we will not reiterate the algorithmic details here. The $O(N)$ polynomial complexity of the BK-GCM method allowed us to perform simulations on large systems and obtain smooth data.

2.2. Characterization of Interfacial Texture

Surface roughness has usually been described using the *solid-on-solid* model [16, 17]. In this model, the surface is described by a single-valued function $h(\vec{r})$ which represents the height of the surface at a position vector $\vec{r}$ on a $(d-1)$-dimensional substrate. The *interface width* is the r.m.s. fluctuation in the height:

$$w^2 = \frac{1}{A}\int d\vec{r}\,\left[h(\vec{r}) - \bar{h}\right]^2 = \frac{1}{A}\int d\vec{r}\;\delta h(\vec{r})^2, \tag{6}$$

where A is the substrate area and $\bar{h}$ is the average height. For a translationally invariant system, we can also write

$$w^2 = \left\langle h(\vec{r})^2\right\rangle - \left\langle h(\vec{r})\right\rangle^2, \tag{7}$$

where the angular brackets denote an ensemble average: $\langle h(\vec{r})\rangle = \bar{h}$. We expect $w^2 \sim L^{2\alpha}$, where α is the *roughness exponent* of the interface [16]. For a self-affine surface, $\alpha = d - d_f$, where d_f is the fractal dimension of the surface.

A more detailed tool for quantifying domain morphologies is the correlation function:

$$C(\vec{r}, \Delta) = \langle\sigma_i\sigma_j\rangle - \langle\sigma_i\rangle\langle\sigma_j\rangle, \tag{8}$$

where $\vec{r} = \vec{r_j} - \vec{r_i}$ and the angular brackets denote an ensemble average. In the isotropic case, $C(\vec{r}, \Delta)$ depends only on the vector magnitude $r = |\vec{r}|$. The correlation length ξ is usually defined as the distance over which $C(r, \Delta)$ decays to (say) 0.2 $\times$ maximum value. The typical GS morphology of the RFIM comprises of compact domains of "up" ($\sigma_i = +1$) and "down" ($\sigma_i = -1$) spins of size $\sim \xi$ separated by rough interfaces. For such a morphology, the small-r behaviour of the correlation function exhibits a *cusp regime* [18]:

$$\bar{C}\,(r) \equiv 1 - C\,(r) \simeq A\,(r/\xi)^{\alpha}\,, \tag{9}$$

where α is the *cusp* or *roughness* exponent. For rough fractal interfaces $0 \leq \alpha < 1$ and the corresponding fractal dimension is $d_f = d - \alpha$. For smooth interfaces, $\alpha = 1$ and is termed the *Porod law* [19].

Scattering experiments measure the structure factor, which is the Fourier transform of the correlation function:

$$S(\vec{k}, \Delta) = \int \mathrm{d}\vec{r}\; e^{i\vec{k}.\vec{r}}\; C(\vec{r}, \Delta), \tag{10}$$

where $\vec{k}$ is the wave-vector of the scattered beam. In the isotropic case $S(\vec{k}, \Delta)$ depends only on the vector magnitude $k = |\vec{k}|$. The short-distance cusp singularity has important implications for the structure factor $S(k)$. It decays with an asymptotic power-law form [20, 21, 22]

$$S(k) \sim \tilde{A}\,(\xi k)^{-(d+\alpha)}\,. \tag{11}$$

The dominant large-k behaviour in Eq. (11) is the *Non-Porod* regime $S(k) \sim (\xi k)^{-(d+\alpha)}$ implying scattering off rough fractal interfaces. In the case of smooth interfaces, $S(k) \sim (\xi k)^{-(d+1)}$ yielding the well known *Porod law*. We emphasize that the correlation-function data yields a more accurate measure of α, as it is obtained by averaging over all domains and interfaces in the system.

3. Numerical Results

The ground states of the RFIM were obtained using the BK-GCM on lattices of size L^3 ($L = 128$). Unless specified otherwise, we employ periodic boundary conditions in all directions. The BK-GCM yields states with 99% overlap with the GS in the first iteration itself, and we observe a mild critical slowing down as $\Delta \to \Delta_c$. All the results have been averaged over 100 realizations of $\{h_i\}$ for a given value of Δ. For the BCC and FCC lattices, we introduce extra sites with $\sigma_i = 0$, converting them to SC lattices with spacing $a/2$. With this procedure, we could use the standard fast Fourier transform routines for evaluating $S(k)$.

We have evaluated the critical disorder strength Δ_c using the fourth order Binder cummulant for the three lattices. These values are: (a) 2.278 ± 0.002 for SC lattice, (b) 3.316 ± 0.002 for BCC lattice and (c) 5.160 ± 0.002 for FCC lattice [14, 23]. It is convenient to define $\delta = (\Delta - \Delta_c)/\Delta_c$, as the critical disorder strength Δ_c is different for the different lattice types. Fig. 1 shows the typical GS morphologies of the RFIM on a SC lattice in (a) the paramagnetic regime ($\delta = 0.08$) and (b) ferromagnetic regime ($\delta = -0.05$). In the paramagnetic regime, the GS has many domains of up and down spins separated by rough interfaces. In the ferromagnetic regime, however, there is a single large cluster of up (down) spins with small impurity clusters of down (up) spins. As a result, it is difficult to extract the interfacial properties in this phase. Therefore, at $\Delta < \Delta_c$, we create interfaces by the following procedure. We apply periodic boundary conditions in the x- and y-directions and fix the spin values at $z = 1, L$ as

$$\begin{aligned} \sigma(x, y, z = 1) &= -1, \\ \sigma(x, y, z = L) &= +1. \end{aligned} \tag{12}$$

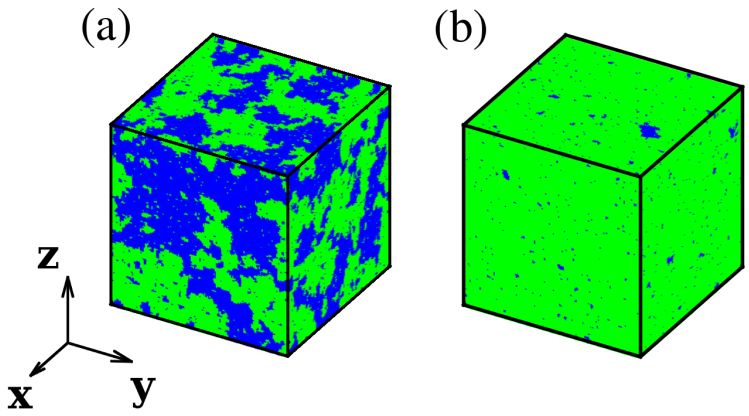

Figure 1. Typical ground state morphologies of the RFIM on a SC lattice of size 128^3 in: (a) the paramagnetic phase ($\delta = 0.08$) and (b) the ferromagnetic phase ($\delta = -0.05$). Green (gray) and blue (black) regions represent up and down spins, respectively.

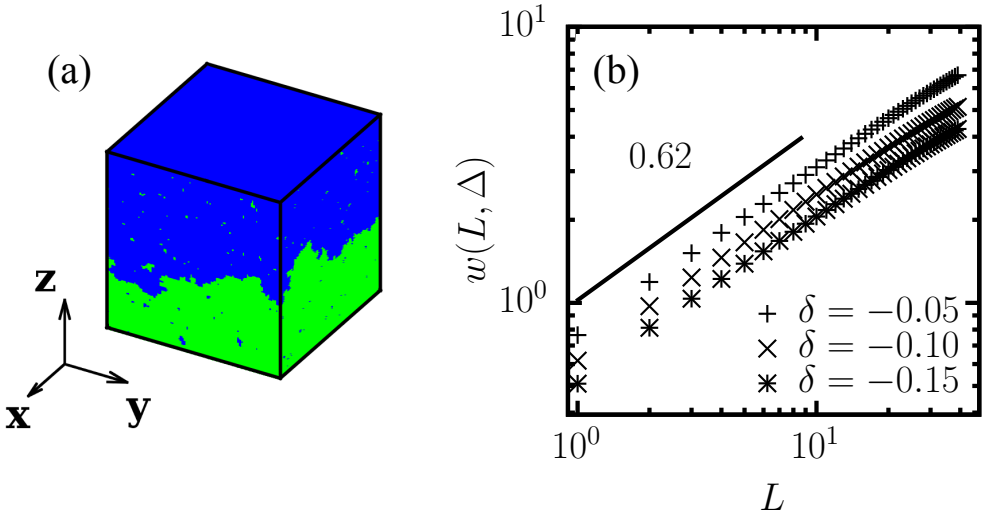

Figure 2. (a) Ground state morphology of the RFIM on a SC lattice of size 128^3 with anti-parallel boundary conditions in the z-direction in the ferromagnetic regime ($\delta = -0.05$). Green (gray) and blue (black) regions represent up and down spins, respectively. (b) Log-log plot of $w(L, \Delta)$ vs. L for the GS of the RFIM on a SC lattice at $\delta = -0.05, -0.1, -0.15$. The slope of the best-fit line to the small-r regime gives $\alpha = 0.62 \pm 0.025$.

Fig. 2(a) shows the typical GS morphology of the RFIM on SC lattice at $\delta = -0.05$ subject to these boundary conditions. There is a well-defined rough interface between up and down domains. In Fig. 2(b), we show the log-log plot of the rms width $w(L)$ vs. L of such interfaces on a SC lattice for $\delta = -0.05, -0.1$ and -0.15. From the slope of the best linear fit, we obtain the roughness exponent $\alpha \simeq 0.62 \pm 0.025$.

We now study the effect of lattice structure on the GS morphologies. In Fig. 3(a), we plot $1 - C(r, \Delta)$ vs. r/ξ on a log-log scale for SC, BCC and FCC lattices in the ferromagnetic regime ($\delta = -0.01$). Our system is not translationally invariant in the z-direction. Therefore,

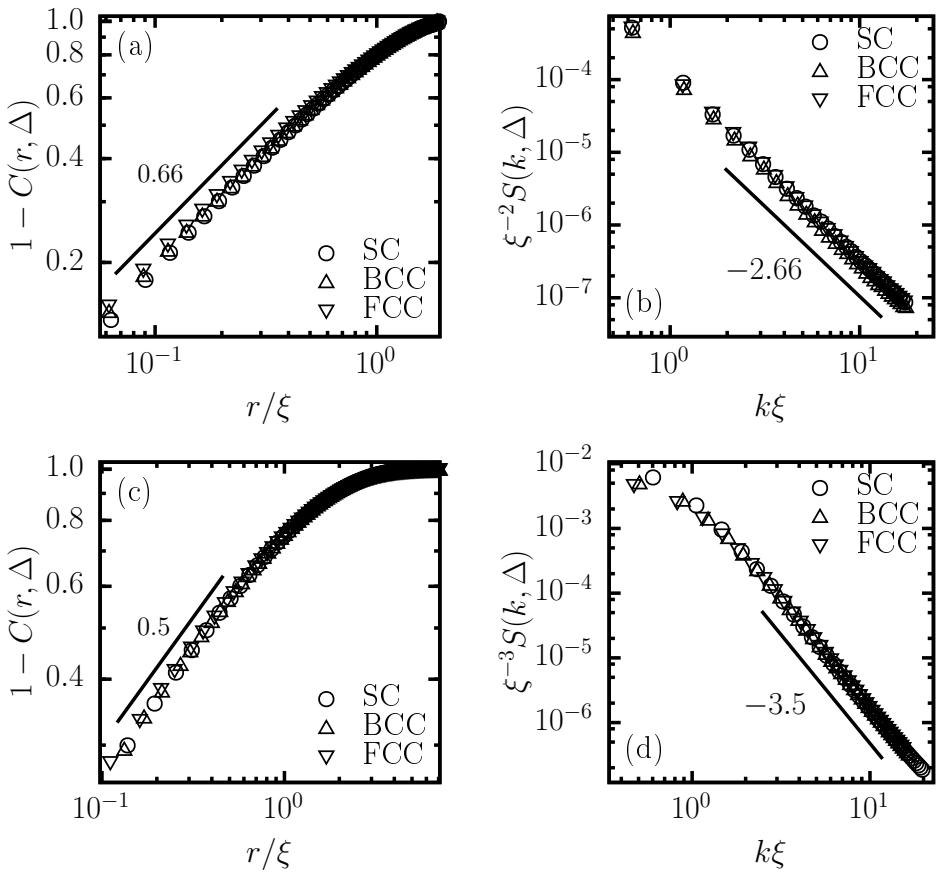

Figure 3. (a) Log-log plot of $1 - C(r, \Delta)$ vs. r/ξ for the RFIM on SC, BCC and FCC lattices with Gaussian disorder in the ferromagnetic regime ($\delta = -0.01$). The corresponding log-log plot of the scaled structure factor $\xi^{-2} S(k, \Delta)$ vs. $k\xi$ is shown in (b). The structure factor shows a non-Porod tail: $S(k, \Delta) \sim k^{-(d+\alpha)}$. Best-fits to the data yield $\alpha = 0.66 \pm 0.02$. (c) Log-log plot of $1 - C(r, \Delta)$ vs. r/ξ for the RFIM on SC, BCC and FCC lattices with Gaussian disorder in the paramagnetic regime ($\delta = 0.08$). The corresponding log-log plot of the scaled structure factor $\xi^{-2} S(k, \Delta)$ vs. $k\xi$ is shown in (d). Best-fits to the data yield $\alpha = 0.5 \pm 0.01$.

we compute the spin-spin correlation function $C(r)$ in the (xy)-plane at $z = \bar{h}$, where $\bar{h}$ is the average height of the interface from the $z = 0$ plane. The linear behaviour of the small-r region yields slightly different values of α for the three lattices in the range $\approx 0.64 - 0.68$. This is consistent with the roughness exponent measured from $w(L)$ in Fig. 2(b). We stress that the correlation function data yields a more accurate measure of α, as it is obtained by averaging over all interfaces in the system. In Fig. 3(b), we plot the scaled structure factor $\xi^{-2} S(k, \Delta)$ vs. $k\xi$ for the correlation functions in Fig. 3(a). It shows a distinct non-Porod behaviour: $S(k) \sim k^{-(d+\alpha)}$. In Figs. 3(c) and (d), we show the corresponding $1 - C(r, \Delta)$ and $S(k, \Delta)$ plots for the SC, BCC and FCC lattices in the paramagnetic regime ($\delta = 0.08$). Best fits to the data yields $\alpha = 0.5 \pm 0.01$, distinct from the ferromagnetic case. Note that the scaling is excellent, indicating that the interfacial textures are unaffected by the lattice structure in the paramagnetic regime.

In Fig. 4(a) we show $1 - C(r, \Delta)$ vs r/ξ on a log-log scale for G, U and B disorder on SC lattice in the paramagnetic regime ($\delta = 0.1$). The corresponding scaled structure factor $\xi^{-3} S(k, \Delta)$ is plotted in Fig. 4(b) on a log-log scale. We find that all the three data sets show excellent

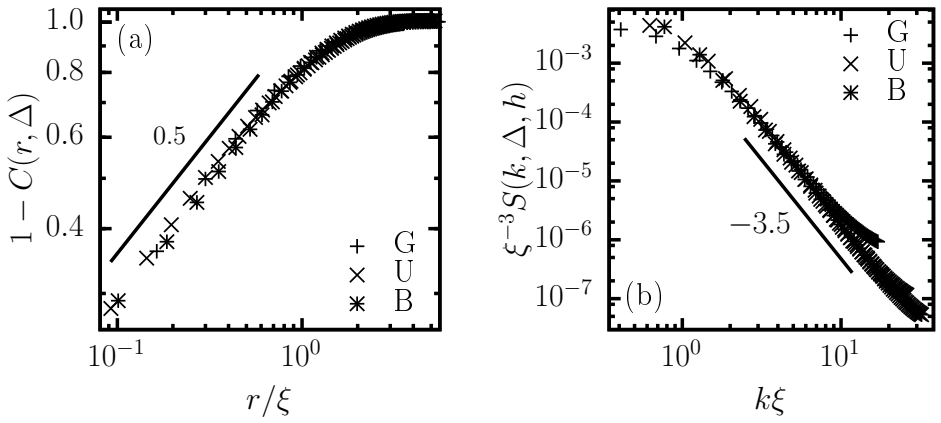

Figure 4. (a) Log-log plot of $1 - C(r, \Delta)$ vs. r/ξ for the RFIM on SC with Gaussian, Uniform and Bimodal disorder in the paramagnetic regime ($\delta = -0.01$). The corresponding log-log plot of the scaled structure factor $\xi^{-2} S(k, \Delta)$ vs. $k\xi$ is shown in (b). The slope of the best-fit line to the data yields $\alpha = 0.5 \pm 0.01$.

collapse. From the best fits to the data we obtain the roughness exponent $\alpha = 0.5 \pm 0.01$. Thus in the paramagnetic phase, the interfacial properties in the RFIM are unaffected by the form of the underlying lattice or disorder.

Finally, we compare our numerical results with the neutron scattering data of randomly diluted antiferromagnets (DAFFs) in a uniform field. They have been some of the most well studied realizations of the RFIM ever since Fishman and Aharony established their equivalence [1, 24, 25, 26]. In Fig. 5 we plot $S(k)$ vs k for the following data sets on a log-log scale. The critical temperature, the experimental temperature and the applied magnetic field strength are provided in the parantheses:
(1) $Fe_{0.46}Zn_{0.64}F_2$ (32.11 K, 32.34 K, 3.0 T) [24];
(2) $Co_{0.35}Zn_{0.65}F_2$ (13.25 K, 2 K, 5.0 T) [25];
(3) $Fe_{0.6}Zn_{0.4}F_2$ (46.13 K, 46.3 K, 2.0 T) [26];
The solid line with slope -4 corresponds to the Porod law, which arises from scattering off smooth interfaces. Clearly, all data sets are non-Porod with slopes greater than -4 indicating that the interfaces separating the phases are fractal. We do not expect to detect the small variations in the slopes due to different lattice structures as the accuracy of the scattering data is limited by the resolution function of the detector.

4. Summary and Discussion

The random field Ising model (RFIM) is simplest example of a system with quenched disorder and provides a framework to study the effects of randomness and disorder on interfacial properties. In this paper we have analysed the influence of (i) different lattice types, viz., simple cubic (SC), body-centered cubic (BCC) and face-centered cubic (FCC) and (ii) different disorder distributions, viz., Gaussian (G), Uniform (U) and Bimodal (B) on the ground state (GS) morphologies of the RFIM. We used a computationally efficient graph-cut procedure to obtain the exact ground states at $T = 0$. We summarize our results as follows:
(a) The GS morphologies of the RFIM comprise of compact domains separated by rough fractal interfaces. We have analyzed these morphologies using spin-spin correlation function $C(r)$ and structure factor $S(k)$.
(b) The correlation function $C(r, \Delta)$ shows a cusp singularity at small-r characterized by the

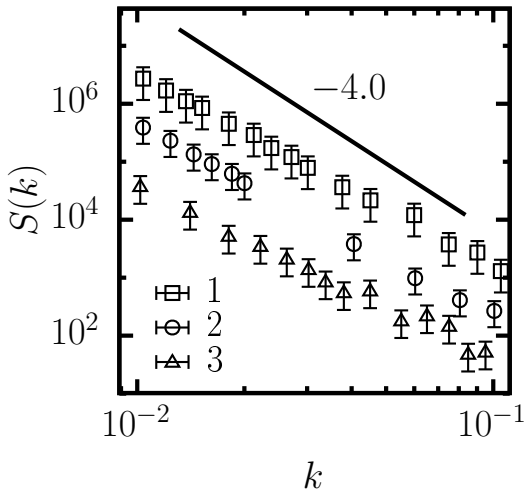

Figure 5. Log-log plot of neutron scattering data of DAFFs: (1) $Fe_{0.46}Zn_{0.64}F_2$ ($T_c = 32.11$ K, $T = 32.34$ K, $H = 3.0$ T) [24]; (2) $Co_{0.35}Zn_{0.65}F_2$ ($T_c = 13.25$ K, $T = 2$ K, $H = 5.0$ T) [25]; (3) $Fe_{0.6}Zn_{0.4}F_2$ ($T_c = 46.13$ K, $T = 46.3$ K, $H = 2.0$ T) [26]; The data sets have been shifted vertically for clarity. The solid line of slope -4 corresponds to Porod scattering from smooth interfaces. All data sets are non-Porod with slope greater than -4, implying scattering off fractal interfaces.

cusp or roughness exponent α. The structure factor shows a corresponding non-Porod behaviour $S(k, \Delta) \sim k^{-(d+\alpha)}$ implying scattering off fractal interfaces.
(c) In the ferromagnetic phase, the roughness exponent $\alpha \simeq 0.66$ for the SC lattice, with minor variations for BCC and FCC lattices. They may be attributed to the different nn environments in the three lattices. The corresponding fractal dimension of the interfaces $d_f = d - \alpha = 2.34 \pm 0.02$.
(d) In the paramagnetic phase, the roughness exponent $\alpha = 0.5 \pm 0.01$, yielding $d_f = d - \alpha = 2.5 \pm 0.01$. The interfacial properties are unaffected by the choice of lattice type or disorder distribition, suggesting that α is a universal exponent in the paramagnetic regime.
(e) Our predictions of fractal interfaces are confirmed in many experimental realizations of the RFIM by analyzing the tail of the structure factor obtained from neutron scattering experiments.

Interfaces in disordered systems have generated a lot of research interest in the past few decades. To understand their behaviour and to manipulate them may be the key to realizing interesting technological applications such as race track memories [10], magnetic logic gates [11], etc. The energy required by a domain of size R to grow or the barrier energy $E_B \sim R^{2-\alpha}$ [8, 9, 14, 23]. The interfacial texture therefore plays a crucial role in growth and relaxation. We believe that our methodologies and analysis may be beneficial from both theoretical and experimental points of view.

Acknowledgments
AB, MK and VB would like to acknowledge partial financial support from Department of Science and Technology (DST), India and Indo-French Centre for Promotion of Advanced Scientific Research (IFCPAR), India.

References
[1] Fishman S and Aharony A 1979 *J. Phys. C: Solid State Phys.* **12** L729.
[2] Schechter M 2008 *Phys. Rev. B* **77** 020401.

[3] Kleemann W, Dec J, Lehnen P, Blinc R, Zalar B and Pankrath R 2002 *Europhys. Lett.* **57** (1) 14.
[4] Vink R L C, Binder K and Löwen H 2006 *Phys. Rev. Lett.* **97** 230603.
[5] Sethna J P, Dahmen K A and Myers C R 2001 *Nature* **410** 242.
[6] Nattermann T and Villain J 1988 *Phase Transitions* **11** 5.
[7] Angls d'Auriac J-C and Sourlas N 1997 *N Europhys. Lett.* **39** 473.
[8] Villain J 1984 *Phys. Rev. Lett.* **52** 1543.
[9] Lai Z W, Mazenko G F and Valls O T 1988 *Phys. Rev. B* **37** 9481.
[10] Thomas L, Moriya R, Rettner C and Parkin S S P 2010 *Science* **330** 1810.
[11] Parkin S S P, Hayashi M and Thomas L 2008 *Science* **320** 190.
[12] Boykov Y and Kolmogorov V 2004 *IEEE Transactions on PAMI* **26** 1124.
[13] Kolmogorov V and Zabih R 2004 *IEEE Transactions on PAMI* **26** 147.
[14] Shrivastav G P, Kumar K, Banerjee V and Puri S 2014 *Phys. Rev. E* **90** 032140.
[15] Shrivastav G P, Krishnamoorthy S, Banerjee V and Puri S 2011 *Europhys. Lett.* **96** 36003.
[16] Barabasi A L and Stanley H E 1995 *Fractal Concepts in Surface Growth* (Cambridge: Cambridge University Press).
[17] Meakin P, Ramanlal P, Sander L M and Ball R C 1986 *Phys. Rev. A* **34** 5091.
[18] Wong P-Z 1985 *Phys. Rev. B* **32** 7417.
[19] Porod G 1982 *Small-Angle X-ray Scattering* Glatter O and Kratky (New York: Academic Press).
[20] Sorensen C M 2001 *Aerosol Sc. Tech.* **35** 648.
[21] Wong P-Z and Bray A J 1988 *Phys. Rev. Lett.* **60** 1344.
[22] Wong P-Z and Bray A J 1988 *Phys. Rev. B* **37** 7751.
[23] Bupathy A, Banerjee V and Puri S 2016 *Phys. Rev. E* **93** 012104.
[24] Belanger D P, Jaccarino V, King A R and Nicklow R M 1987 *Phys. Rev. Lett.* **59** 930.
[25] Hagen M, Cowley R A, Satija S K, Yoshizawa H, Shirane G, Birgeneau R J and Guggenheim H J 1983 *Phys. Rev. B* **28** 2602.
[26] Belanger D P, King A R and Jaccarino V 1985 *Phys. Rev. B* **31** 4538.